

## **Composition of curvilinearly extendable tubular scissor mechanisms**

Seita Tsuda<sup>a,\*</sup>, Junpei Kohno<sup>b,1</sup>, Yoshihiro Nakahara<sup>c</sup>, Makoto Ohsaki<sup>d</sup>

<sup>a</sup> *Department of Architecture, Okayama Prefectural University, 111 Kuboki, Soja 719-1197, Japan*

<sup>b</sup> *Graduate school of Design, Okayama Prefectural University, 111 Kuboki, Soja 719-1197, Japan*

<sup>c</sup> *Department of Craft and Industrial Design, Okayama Prefectural University, 111 Kuboki, Soja 719-1197, Japan*

<sup>d</sup> *Department of Architecture and Architectural Engineering, Kyoto University, Kyoto-Daigaku Katsura, Nishikyo, Kyoto 615-8540, Japan*

### **Abstract**

Scissor mechanisms are used as deployable structures in industrial products, architecture, and aerospace structures. In general, tubular scissor mechanisms (TSMs), composed of scissor-like elements on their surrounding facets, extend collinearly to serve as lifters, masts, and bridges. Furthermore, curved TSMs can form circular arches to serve as spatial frames and space antennas. However, previous studies proposed limited configurations of TSM models and did not present detailed geometrical formulations. This paper presents new compositions of curved TSMs that can extend by winding two-dimensionally or twisting three-dimensionally. Detailed geometrical formulations of the scissor-like elements were analytically derived to generate a variety of extended shapes. In addition to the numerical simulations using 3D CAD, physical models were assembled to verify their deployability considering realistic sizes of bars and joints. This work widens the deployability of extendable scissors mechanisms, which will eventually broaden the usage of this structure in practical applications.

### **Keywords**

Deployable structure, Scissor mechanism, Tubular structure, Mobile structure, Pantograph, Arches, Geometric design

---

\* Corresponding author. Tel: +81 866 94 2016, E-mail address: tsuda@dgn.oka-pu.ac.jp (S. Tsuda)

<sup>1</sup> Currently, Nikken Sekkei LTD.

## 1. Introduction

Deployable structures, which can easily and rapidly transform their shape as needed, have been utilized extensively in deployable shelters, retractable roofs, space antennas, and especially in temporary and mobile structures. Scissor mechanisms are popular deployable structures in industrial products in architectural and aerospace applications. Scissor structures consist of several scissor-like elements (SLEs), each of which consists of two rigid bars connected at the intermediate point of the bars using a pivot—a rotational joint around an axis perpendicular to the plane containing two bars. By connecting several SLEs in a row with revolute joints at the ends of corresponding bars, a single-degree-of-freedom (single-DOF) unidirectionally extending planar scissor mechanism can be assembled. By arranging such planar scissor mechanisms in two or three directions, spatial mechanisms for use in specific applications, such as roof structures and space antennas, can be developed (Pinero, 1965). Pantographic mechanisms such as lifters, bridges, and mast structures that extend one-dimensionally are also widely used. Escrig (1985) proposed a variety of scissor mechanisms. Many researchers, including Hanor and Levy (2001) and Maden et al. (2019), have reviewed and categorized the development of scissor mechanisms.

This paper focuses on pantographic scissor mechanisms and devises a novel assembly that extends with a compound curve. When  $n$  SLEs are connected to form a closed loop, it generates a polyhedron with  $n + 2$  facets ( $n$  facets with SLEs and two vacant facets). Connecting such polyhedral mechanisms in an extended manner creates a tubular scissor mechanism (TSM), which is internally vacant and enclosed by  $n$  facets with the SLEs surrounding it. Many researchers have investigated TSMs that extend collinearly, as shown in Fig. 1(a). Escrig and Valcarcel (1993) composed a variety of collinearly extendable assemblies. Atake (2000) proposed several design ideas about prismatic masts and bridges; however, they did not provide theoretical explanations. De Temmerman (2007) proposed prismatic scissor masts using

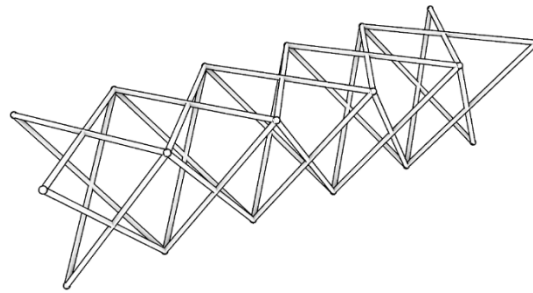
angulated bars, which extend rapidly compared to straight bars.

Scissor mechanisms are usually assembled as single-DOF mechanisms, and thus, they become load-bearing structures by adding one additional constraint. However, pantographic scissor structures generally do not have sufficient stiffness as columns (Raskin, 1998). Kwan et al. (1993) and You and Pellegrino (1996) inserted active and passive cables to stiffen pantographic masts. De Temmerman (2007) evaluated the structural performance of passively stiffened scissor masts that were exposed to realistic wind loads through structural analysis. Glisic (2013) presented a smart pantograph mast equipped with sensors and actuators.

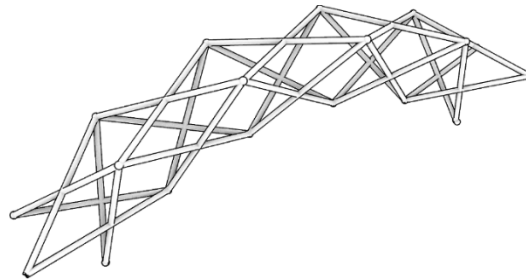
A curved scissor mechanism with straight bars, generally called a polar scissor unit, can be created by assigning a pivot in a position other than the center of the bars. Deployable barrel vaults are usually composed of polar scissor units along their span direction and translational scissor units along their longitudinal direction (Alegria Mira et al., 2014; Langbecker and Albermani, 2001). Considering TSMs composed of polar units, Escrig (1985) and Escrig and Valcarcel (1993) proposed a sort of curved triangular TSM as shown in Fig. 1(b). Although these studies do not describe the details of the mechanisms, the structures appear to be composed of identical SLEs. This means that the mechanism extends with a single curve.

Planar scissor mechanisms with compound curves can be created by assigning pivots differently in each SLE (Babaei and Sanaei, 2009; Rosenberg, 2010). For example, Maden et al. (2011) proposed a bridge-like mechanism with a compound curve by arranging in parallel two identical planar–curved scissor mechanisms and connecting them with rigid straight bars. However, this kind of composition can form only two-dimensional transformation. Similarly, the curved TSM proposed by Escrig can transform two-dimensionally with a single curve. Conversely, in this study, we developed curved TSMs that are composed of a variety of polar and translational units on their surrounding facets. This feature enables extendable TSMs to transform, winding not only two-dimensionally but also twisting three-dimensionally.

The remainder of this paper is organized as follows. Section 2 presents the basic geometry of planar scissor mechanisms composed of polar units. Section 3 presents the compositions of TSMs that extend with a two-dimensional winding and discusses their deployment performance based on the arrangement of the components. Section 4 presents the compositions of TSMs that deploy with three-dimensional twisting. In addition, some small physical models were assembled to verify mobility. Although this paper mainly discusses the geometry of the assemblies without regard to the finite size of the bars and connections, a straightforward design of the joints is presented to help with the fabrication of physical models.



(a) Collinear

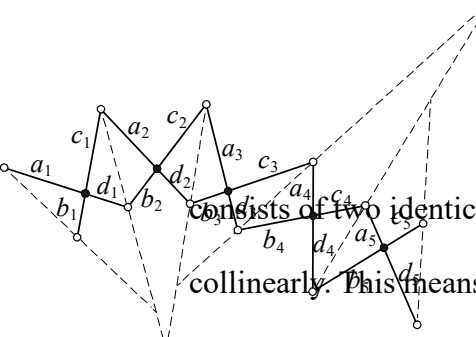


(b) Curved

**Fig. 1.** Typical triangular TSMs.

## 2. Planar scissor mechanisms

The geometrical properties of planar scissor mechanisms are analytically discussed in this section. Note that the TSMs described in this study include only straight bars. When an SLE



consists of two identical bars connected with a pivot at the center of each bar, the SLE deploys collinearly. This means that the unit lines—imaginary lines that pass through two end hinges—are always parallel, as shown in Fig. 2(a). This type of SLE is referred to as a translational unit. By symmetrically shifting the pivot from the center toward its ends, the SLE is curvilinearly deployed. As a result, the unit lines intersect at a concurrency point, as shown in Fig. 2(b). This type of SLE is known as a polar unit.

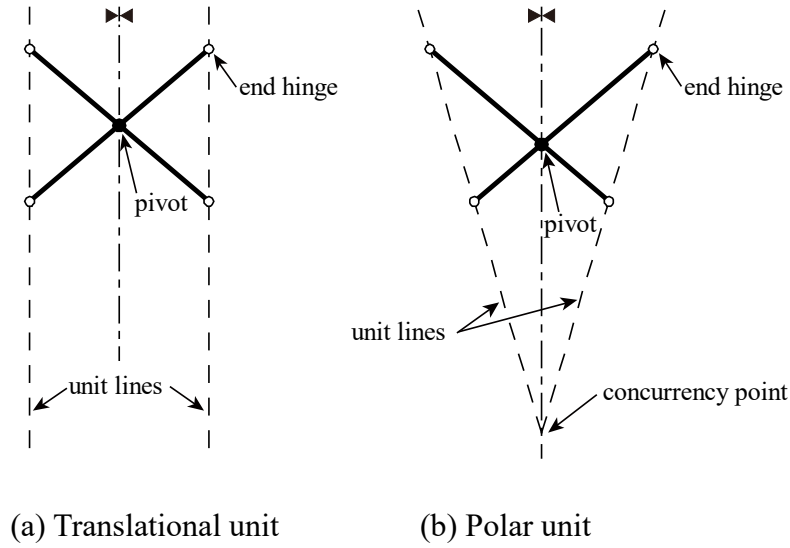


**Fig. 2.** Representative SLE unit showing symmetry.

(The symbol  $\blacktriangleleft$  represents the axis of symmetry).

Figure 3 illustrates a scissor mechanism assembled with several types of polar units. The symbols "●" and "○" represent the pivot and end hinge joints, respectively. For compatibility between adjacent units, the following equation should be satisfied:

$$a_{i+1} + b_{i+1} = c_i + d_i, \quad (1)$$

which is called Escriq's constraint. This constraint also ensures that the mechanism folds into a fully compact configuration (into a line if the finite sizes of the bars and connections are neglected).

**Fig. 3.** Scissor mechanism with different polar units.

If a scissor mechanism is composed of SLEs with the same pivot positions, the scissor mechanism forms a single circular curve, as shown in Fig. 4. In contrast, the scissor mechanism extends with a compound curve if each SLE has a different pivot position, as shown in Fig. 5.

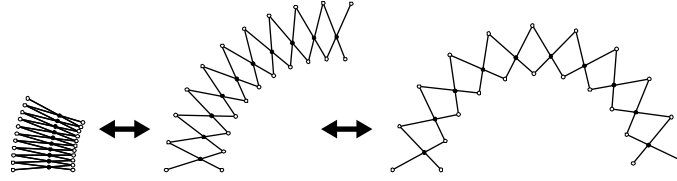


**Fig. 4.** Polar scissor mechanism with a single curve.

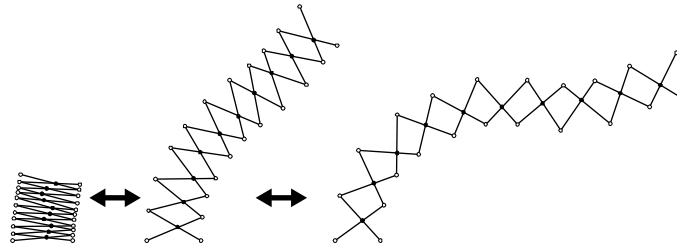


**Fig. 5.** Polar scissor mechanism with a compound curve.

Each SLE is assembled to be symmetrical, as shown in Fig. 2(b), and thus satisfies

$$a_i = c_i \text{ and } b_i = d_i. \quad (2)$$

The solution of Eqs. (1) and (2) implies that all the bars in the mechanism need to have the same length, which is hereafter denoted as  $L$ .

Figure 6 illustrates the definitions of the variables for a polar SLE (pSLE). To specify the position of the pivot, the pivot eccentricity is defined by  $e$  ( $0 < e < 1$ ). The total length of each bar is  $L$ , the semi-length of the bars on the left (the distance from A to P) is  $eL$ , and that of the bars on the right (the distance from P to D) is  $(1-e)L$ . Thus,  $e = 0.5$ , when the pivot is located at the center of the bars. The deployment angle of the two bars ( $\angle APC$ ) is denoted as  $2\varphi$ . The

value of  $\varphi$  is 0 in the completely folded state and  $90^\circ$  in the fully deployed state. The thickness of the SLE (the distance from A to B) is denoted by  $t$ . The heights on the left (A to C) and right (B to D) are denoted as  $h$  and  $\tilde{h}$ , respectively.

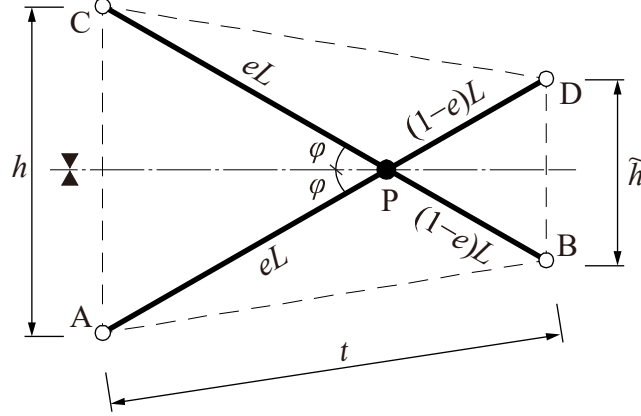


**Fig. 6.** Definitions of variables of a pSLE.

Using the cosine theorem for the triangles APB and APC, the following equations are obtained:

$$t^2 = e^2L^2 + (1 - e)^2L^2 - 2e(1 - e)L^2 \cos(\pi - 2\varphi), \quad (3)$$

$$h^2 = 2e^2L^2 - 2e^2L^2 \cos 2\varphi. \quad (4)$$

Eliminating  $\varphi$  from Eqs. (3) and (4) results in

$$t^2 + \frac{1 - e}{e}h^2 = L^2. \quad (5)$$

A polar scissor mechanism with a compound curve is obtained by assembling a chain of pSLEs with different  $e$  values. The variables related to the  $i$ th unit are indicated by the subscript  $i$  as  $A_i$ ,  $B_i$ ,  $C_i$ ,  $D_i$ ,  $P_i$ ,  $e_i$ ,  $h_i$ , and  $\tilde{h}_i$ . Because  $L$  is constant and  $t$  has the same value throughout the mechanism, the ratio of  $h$  in the  $j$ th unit to that in the  $i$ th unit is obtained from Eq. (5) as

$$\frac{h_j}{h_i} = \sqrt{\frac{1 - e_i}{e_i} \frac{e_j}{1 - e_j}}. \quad (6)$$

As the ratio is expressed only by  $e_i$  and  $e_j$ , it remains constant during deployment. In addition, the height ratio between the left and right sides,  $\tilde{h}_i/h_i$ , is constant because the bars are straight. Therefore, the height ratios among all the units are constant during the deployment. The method of composing curved TSMs is developed exploiting these properties in Section 3.

The constants and parameters of the mechanism in Fig. 5 are as follows: the total number of units is 10;  $L = 2000$  mm; the values of  $t$  are 1990, 1800, and 1500 mm from the left to the right, respectively. The values of  $e_i$  are shown in Table 1.

**Table 1.** Pivot eccentricity of mechanism in Fig. 5.

$i$	$e_i$
1	0.560
2	0.600
3	0.635
4	0.500
5	0.585
6	0.610
7	0.460
8	0.385
9	0.470
10	0.600

### 3. Two-dimensionally curved TSM

#### 3.1. Composition of a curved TSM unit

Figure 7 shows the unit of a rectangular TSM. Imaginary planes and edges are depicted in the figure to define and clarify the components. Two identical pSLEs are set in parallel, composing the “side planes” (gray). These pSLEs are connected to another pair of SLEs, which compose the “connecting planes” (red). As a result, two vacant rectangular planes called “cross-sections” appear. The distance between two side planes, called the width of the TSM unit, is denoted as  $w$ . Note that the side planes and connecting planes should connect at right angles using appropriate connections during the deployment process so as not to increase the DOF of the TSM unit. The details of such connections are described in Section 4.2.

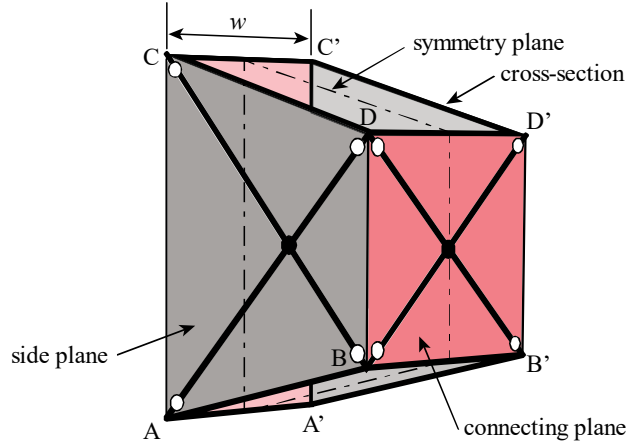


**Fig. 7.** Rectangular-TSM unit.

The configuration of SLEs on the connecting planes is essential to compose the TSM as a stress-free mechanism. Two types of TSM units are described below to explain the deployability scheme. The first includes conventional two-bar SLEs on the connecting planes. The geometric nets and cross-sections of the rectangular TSM are shown in Fig. 8. The deployment angles of the two bars on the connecting planes are denoted as  $2\theta$  (on the left) and  $2\tilde{\theta}$  (on the right). Hereafter, the deployment status of a TSM unit is defined by  $\theta$  ( $\theta = 0$ : completely folded state,  $\theta = \pi/2$ : fully deployed state). The figure shows that  $\theta$  and  $\tilde{\theta}$  exhibit different values during the deployment, and the cross-section forms a trapezoidal configuration.

In addition to the assembly process of a unit, as shown in Fig. 8, we need to evaluate TSMs composed of several units. For example, suppose that more than two TSM units with different pivot eccentricities are connected. Then, the assembled structure will have internal forces during the deployment process because the widths of adjacent units do not match with each other. Thus, the assembly becomes a stress-free mechanism only when all TSM units have identical pivot-eccentricities, such as Escrig's triangular TSM, as shown in Fig. 1(b).

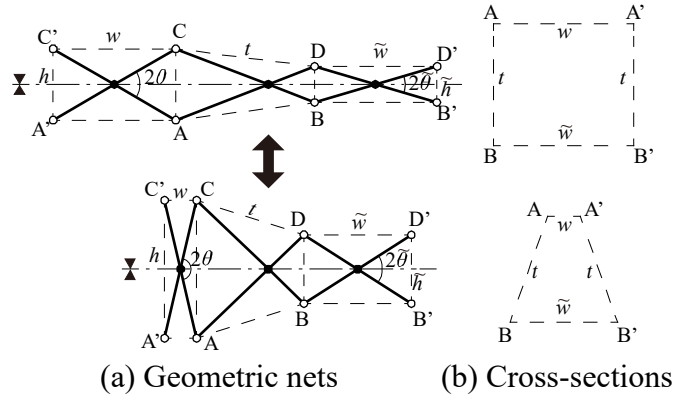


**Fig. 8.** Deployment of a TSM unit with conventional SLEs on connecting planes.

(The other side of the pSLE is omitted.)

Using multiple SLEs on the connecting planes, as shown in Fig. 9, can avoid the problems mentioned above. The value of  $e$  is  $2/3$  in the figure, which means that the  $h/\tilde{h}$  ratio is always 2. Thus, by assigning two identical SLEs longitudinally on the left side and one same SLE on the right side, one can create a stress-free mechanism with a rectangular cross-section during deployment.

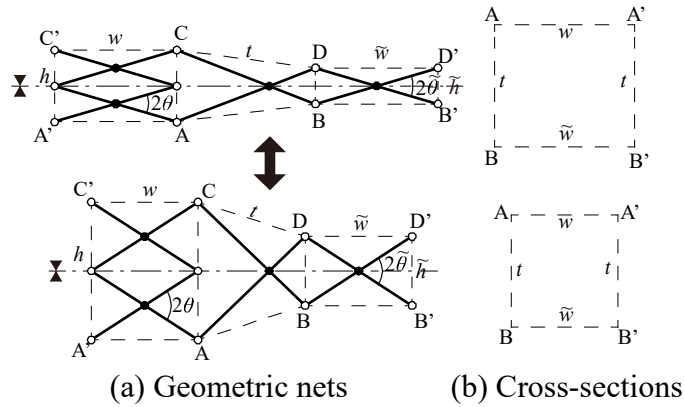


**Fig. 9.** Deployment of a TSM unit with multiple SLEs on the connecting planes.

Such multiple SLEs on the connecting planes are called “mSLEs” hereafter. If a pivot divides a bar with a ratio of positive integers, one can compose an mSLE using entirely identical SLEs. Otherwise, the bar lengths of the mSLEs require adjustment according to the pivot eccentricities of the pSLEs. Figure 10 shows a list of such mSLEs, which can be composed not

only by longitudinal arrangements but also by transverse arrangements. The figure shows mSLEs from three rows (in the transverse direction) to three tiers (in the longitudinal direction). The mSLE types are named X3r, X2r, X1, X2t, and X3t. All the mSLEs types are symmetric with respect to both the horizontal and vertical axes. Some types of these compositions have already been utilized to assemble dome frames (You and Chen, 2012). The relationship between  $e$  and the mSLEs types is discussed in Section 3.3.

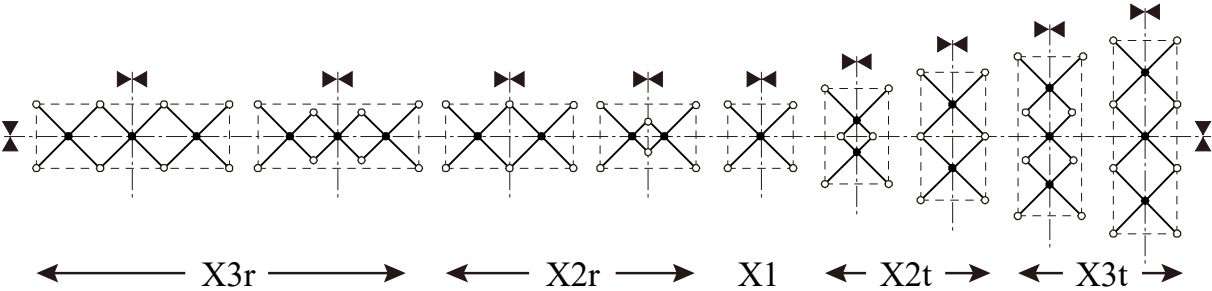


**Fig. 10.** Types of mSLEs.

(Models with more than four tiers and four rows are omitted).

The bar lengths of the mSLEs are defined as follows: the total bar length from an end hinge to the vertical axis of symmetry is  $l/2$ , and the total bar length from an end hinge to the horizontal axis of symmetry is  $(1 + \beta)l/2$ . For example, Fig. 11 illustrates the lengths of types X3t and X3r. This definition leads to a distinct classification: if  $\beta = 0$ , the mSLE is a conventional two-bar unit; if  $\beta > 0$ , the mSLE is composed of a longitudinal arrangement with multiple tiers; if  $\beta < 0$ , the mSLE is composed of a transverse arrangement with multiple rows. Figure 12 shows some cases of mSLEs with different  $\beta$  values. Table 2 shows the range of  $\beta$  according to the composition of the mSLEs.

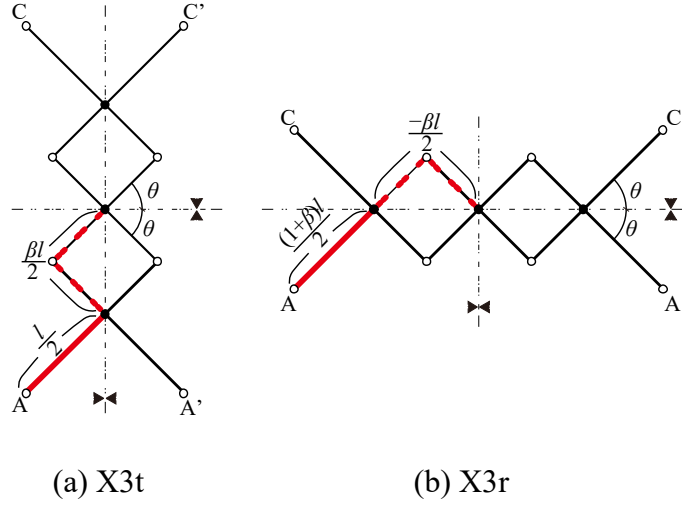


**Fig. 11.** Definitions of lengths of bars of mSLEs.

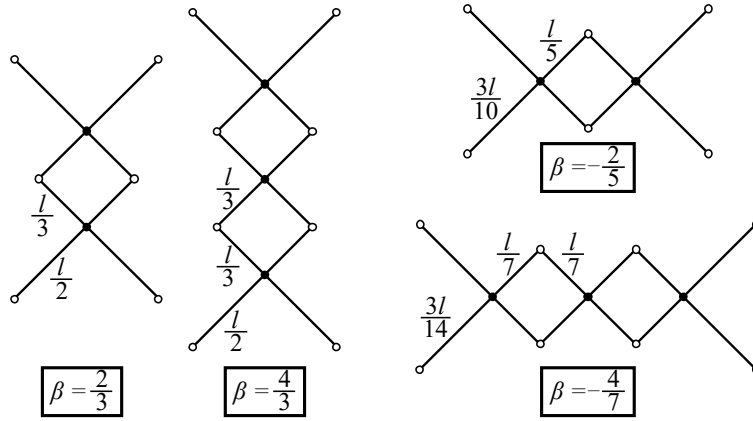


**Fig. 12.** Examples of mSLEs with different  $\beta$ .

**Table 2.** Range of  $\beta$  according to the composition of mSLEs.

Type	Range of $\beta$
X4r	$-3/4 \leq \beta < -2/3$
X3r	$-2/3 \leq \beta < -1/2$
X2r	$-1/2 \leq \beta < 0$
X1	$\beta = 0$
X2t	$0 < \beta \leq 1$
X3t	$1 < \beta \leq 2$
X4t	$2 < \beta \leq 3$

From the above definition, the width and height of the mSLE are expressed as follows:

$$w = l \cos \theta, \quad (7)$$

$$h = (1 + \beta)l \sin \theta. \quad (8)$$

If  $l$  is set to be equal throughout the assembly, the widths of all the TSM units become equal under the same  $\theta$ . In addition, the ratio of the  $j^{\text{th}}$  unit's height to the  $i^{\text{th}}$  unit's height is expressed by Eq. (8) as follows:

$$\frac{h_j}{h_i} = \frac{1 + \beta_j}{1 + \beta_i}, \quad (9)$$

which is constant during the deployment. Furthermore, Eq. (6), obtained under the condition that  $L$  is identical throughout all the pSLEs, ensures that the height ratios among any units are constant. Therefore, one can compose a TSM whose cross-sections remain rectangular during the deployment by using identical  $L$  in all the pSLEs and equal total bar length,  $l$ , in all the mSLEs. The value  $\beta_i$  can be set arbitrarily; however, the value affects the cross-section configuration, which will be discussed in the following section.

### 3.2. Deployment of a curved TSM

This section evaluates the change in the cross-sectional shapes during the deployment process.

First, the ratio  $l$  to  $L$  is set to  $k$  as follows:

$$l = kL. \quad (10)$$

The ratio of the width to thickness,  $w/t$ , can be obtained from Eqs. (5), (7), (8), and (10).

$$\frac{w}{t} = k \sqrt{\frac{1 - \sin^2 \theta}{1 - \frac{1-e}{e} k^2 (1 + \beta)^2 \sin^2 \theta}}. \quad (11)$$

Hereafter,  $w/t$  is called the “width–thickness ratio.” The value varies during the deployment because it contains  $\theta$ .

The ratio of  $h$  in the  $j$ th unit to that in the  $i$ th unit is constant, as described in Eqs. (6) and (9), which leads to

$$\beta_j = (1 + \beta_i) \sqrt{\frac{1 - e_i}{e_i} \frac{e_j}{1 - e_j}} - 1. \quad (12)$$

Therefore, we can determine only one value of  $\beta$  arbitrarily among all the mSLEs, and  $\beta$  in the other mSLEs is calculated using Eq. (12).

Let us find the condition when the cross-section maintains similar rectangles throughout the deployment. This is the case when the width–thickness ratio in Eq. (11) is constant for any value of  $\theta$ . This condition is achieved when the following equation is satisfied:

$$\frac{1-e}{e}k^2(1+\beta)^2 = 1. \quad (13)$$

Thus, the value  $\beta_s$ , which makes the cross-sections as similar rectangles throughout the deployment, is obtained as

$$\beta_s = \sqrt{\frac{e}{1-e}k} - 1. \quad (14)$$

The value  $\beta_s$  in each unit is determined uniquely by this equation.

Figure 13 shows the width–thickness ratio of seven TSM units ( $k = 1$ ,  $e = 2/3$ ,  $\beta = -1, 0.333, 0.38, 0.414214, 0.45, 0.6$ , and  $1.0$ ) during the deployment. From Eq. (14),  $\beta_s = \sqrt{2} - 1 \approx 0.414214$ . The figure shows that if  $\beta$  is smaller than  $\beta_s$ , the width–thickness ratio decreases continuously. On the contrary, if  $\beta$  is larger than  $\beta_s$ , the width–thickness ratio increases continuously.

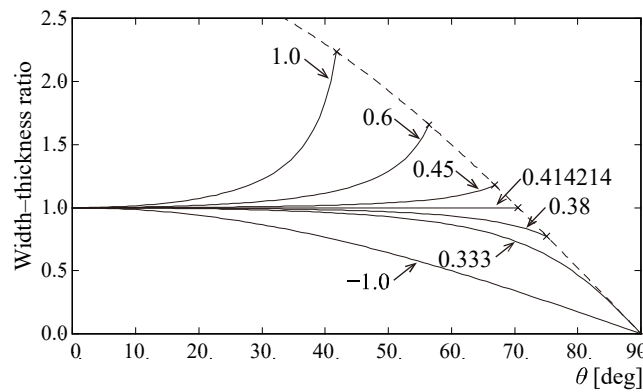


**Fig. 13.** Width–thickness ratio during the deployment.

(Horizontal axis: deployment angle  $\theta$  ( $^\circ$ ); vertical axis: width–thickness ratio  $w/t$ ;  $\times$  represents the limit of extension; dashed line illustrates the envelope of limit for continuously varied  $\beta$ .)

The assembly can extend until either the pSLEs or mSLEs reach the fully deployed state. When a pSLE is fully deployed, the deployment angle of the bars on the side planes,  $\varphi_i$ , equals  $90^\circ$ . Because  $h_i = 2e_iL$  in this state, the following equation can be obtained from Eqs. (8) and (10), as follows:

$$\sin \theta = \frac{2e}{(1 + \beta)k}. \quad (15)$$

Because  $\theta$  needs to be between  $0^\circ$  and  $90^\circ$ ,  $\beta$  must satisfy the following constraint equation:

$$\beta \geq \frac{2e}{k} - 1 := \beta_L \quad (16)$$

If  $\beta$  is equal to its lower bound  $\beta_L$ , both pSLEs and mSLEs are extended simultaneously to a fully deployed state. This means that the TSM unit can extend to one straight line if the sizes of the bars and connections are neglected. If  $\beta > \beta_L$ , the pSLE reaches the fully deployed state, whereas the mSLE remains partially deployed. The limit deployment angle of an mSLE,  $\theta_i^{\text{MAX}}$ , can be obtained from Eq. (15) as

$$\theta_i^{\text{MAX}} = \sin^{-1} \left( \frac{2e_i}{(1 + \beta_i)k} \right). \quad (17)$$

This limit status is shown with the symbol  $\times$  in Fig. 13; the envelope of limit for continuously varied  $\beta$ , computed from Eqs. (11) and (17), is also illustrated with the dashed line. If  $\beta < \beta_L$ , Eq. (15) has no solution: In other words, the pSLE is partially deployed when the mSLE is fully deployed. The limit deployment angle of the pSLE,  $\varphi_i^{\text{MAX}}$ , can be obtained from Eqs. (4), (8), and (10) as

$$\varphi_i^{\text{MAX}} = \frac{1}{2} \cos^{-1} \left( 1 - \frac{(1 + \beta)^2 k^2}{2e^2} \right). \quad (18)$$

The limit deployment state of the entire TSM is determined by the unit that has the minimum  $\theta_i^{\text{MAX}}$ . However, it is unnecessary to calculate  $\theta_i^{\text{MAX}}$  in all units because the dominant pSLE must have the maximum  $t$  when fully deployed, i.e., when  $\varphi_i = 90^\circ$ . If the pivot is in the

center of the bars ( $e = 0.5$ ), the thickness is reduced to zero. If the pivot is closest to the end hinge, that is, the absolute value of  $(e - 0.5)$  is the largest, the pSLE has the maximum  $t$  and thus determines the limit state of the entire TSM.

### 3.3. Composition of rectangular TSM

This section describes the relationship between the pivot eccentricities and the type of mSLEs. For simplicity, we focus on the TSM in which the cross-sections form similar rectangles during the deployment. To compose a TSM with a large curvature, i.e., pivots are located close to the ends of the bars, the mSLEs should be assembled with many rows or tiers. However, such a mechanism is complicated and eventually increases the number of bars and hinges. Therefore, it is desirable to limit the eccentricity of the pivot.

The range of  $e$  according to the composition of the mSLEs can be specified using Eq. (14) and Table 2. For example, the composition of X2t requires  $0 < \beta \leq 1$ , giving

$$\text{2-tiers: } \frac{k^2}{1+k^2} < e \leq \frac{4k^2}{1+4k^2}. \quad (19)$$

The composition of X2r requires  $-1/2 \leq \beta < 0$ , giving

$$\text{2-rows: } \frac{k^2}{4+k^2} \leq e < \frac{k^2}{1+k^2}. \quad (20)$$

Similarly, the range of  $e$  in  $n$ -tiers and  $m$ -rows can be obtained as follows:

$$\text{\textit{n}-tiers: } \frac{(n-1)k^2}{1+(n-1)^2k^2} < e \leq \frac{n^2k^2}{1+n^2k^2}, \quad (21)$$

$$\text{\textit{m}-rows: } \frac{k^2}{m^2+k^2} \leq e < \frac{k^2}{(m-1)^2+k^2}. \quad (22)$$

Table 3 shows the range of  $e$  according to the type of mSLEs and  $k$ . Only one side of the boundary is mentioned in the table for simplicity. If  $k = 1$ , for example, type X1 can be possible only when  $e = 0.5$ ; for X2t, X3t, and X4t,  $e$  must be in the range of 0.5–0.8, 0.8–0.9, and 0.9–

0.941, respectively; for X2r, X3r, and X4r,  $e$  must be in the range of 0.2–0.5, 0.1–0.2, and 0.0588–0.1, respectively.

**Table 3.** Range of  $e$  according to the type of mSLE and  $k$ .

$k$	X4r	X3r	X2r	X1	X2t	X3t	X4t
1/2	0.0154–	0.0270–	0.111–	0.2	–0.5	–0.692	–0.8
2/3	0.0270–	0.0471–	0.1–	0.308	–0.640	–0.8	–0.877
4/5	0.0385–	0.0664–	0.138–	0.390	–0.719	–0.852	–0.911
1	0.0588–	0.1–	0.2–	0.5	–0.8	–0.9	–0.941
5/4	0.0890–	0.148–	0.281–	0.610	–0.862	–0.934	–0.962
3/2	0.123–	0.2–	0.360–	0.692	–0.9	–0.953	–0.973
2	0.2–	0.308–	0.5–	0.8	–0.941	–0.973	–0.985

Table 4 shows  $\beta_s$  and the types of mSLEs on the left connecting plane of the TSM in Fig. 5. Three cases ( $k = 0.5, 1, 2$ ) are listed in the table. The limit deployment angle  $\theta^{\text{MAX}}$  is  $76.8^\circ$ , determined in the 3rd unit. The compositions of the mSLEs on the right connecting plane are omitted in the table, which can be obtained using the pivot eccentricities,  $1 - e$ . Figure 14 shows the extended rectangular TSM with  $k = 1$  and  $\beta_s$ . Similar models have been designed in previous works (Maden et al., 2011). The difference is that their models comprise straight bars on connecting planes, which means that the widths of the assemblies do not change. By contrast, our TSMs can produce various cross-sections.

**Table 4.** Composition of mSLEs in Fig. 5 and Table 1.

$k$		0.5	1	2
$l$		1000	2000	4000
$i$	$e_i$	$\beta_s$ (type)	$\beta_s$ (type)	$\beta_s$ (type)
1	0.560	1.256 (X3t)	0.128 (X2t)	–0.436 (X2r)
2	0.600	1.449 (X3t)	0.225 (X2t)	–0.388 (X2r)
3	0.635	1.638 (X3t)	0.319 (X2t)	–0.341 (X2r)
4	0.500	1.000 (X2t)	0.000 (X1)	–0.500 (X2r)
5	0.585	1.375 (X3t)	0.187 (X2t)	–0.406 (X2r)
6	0.610	1.501 (X3t)	0.251 (X2t)	–0.375 (X2r)
7	0.460	0.846 (X2t)	–0.077 (X2r)	–0.539 (X3r)
8	0.385	0.582 (X2t)	–0.209 (X2r)	–0.604 (X3r)
9	0.470	0.883 (X2t)	–0.058 (X2r)	–0.529 (X3r)
10	0.600	1.449 (X3t)	0.225 (X2t)	–0.388 (X2r)

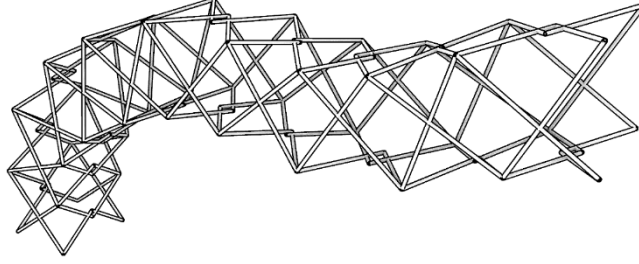


**Fig. 14.** Rectangular TSM with  $k = 1$ .

### 3.4. Composition of triangular TSM

Even though we have only discussed the TSMs with rectangular cross-sections, the TSMs with triangular cross-sections can be designed in the same way. Figure 15 shows a unit of a triangular TSM, which consists of two identical pSLEs and an mSLE. Figure 16 illustrates the change in the cross-sectional shapes according to  $k$  and  $\beta$ . To assemble a TSM with an equilateral-triangular cross-section throughout the deployment, the value  $k$  must be set to one, i.e.,  $L = l$ , and the value  $\beta$  must be  $\beta_s$ , which is derived from Eq. (14). If  $k \neq 1$  and  $\beta = \beta_s$ , the cross-sections consistently outline similar isosceles-triangles. Furthermore, if  $\beta \neq \beta_s$ , the cross-sections form isosceles triangles, while their internal angles continuously vary. Figure 17 shows the extended triangular TSM. The pSLEs are assembled with  $e$  in Table 1,  $k = 1.0$ , and  $\beta_s$  calculated using Eq. (14). Such a triangular-TSM with a compound curve can be designed by modifying the composition of TSM proposed by Escrig (1985). As with rectangular-TSMs, the cross-sectional shape of triangular-TSMs can be tuned as desired because they are not composed of straight bars.

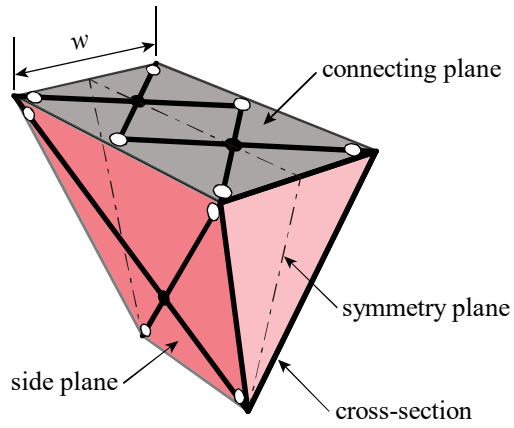


**Fig. 15.** Triangular-TSM unit.

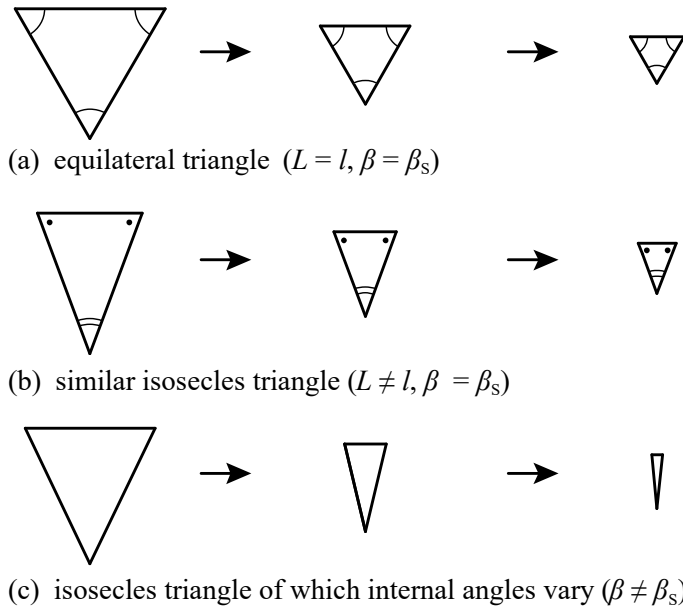


**Fig. 16.** Variation of cross-sectional shapes in triangular TSMs.

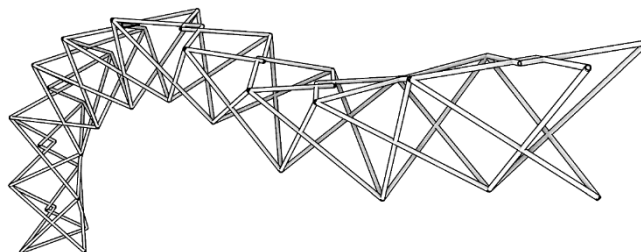


**Fig. 17.** Triangular TSM with  $k = 1$ .

## 4. Three-dimensionally curved TSM

### 4.1. Composition of twisting TSM

Because a rectangular TSM has two parallel side planes, the mechanism has a plane of symmetry and thus transforms by winding two-dimensionally. Likewise, a triangular TSM transforms by winding two-dimensionally because the assembly is symmetric, although its side planes are not located in the same plane. Thus, the mechanisms described in the previous sections are sufficient for a simple two-dimensional extension.

This section describes the composition of the TSMs that transform by twisting three-dimensionally, similar to a spiral staircase. Such TSMs can be obtained by rotating the positions of the side planes and connecting planes in the middle part of the TSM. In other words, they can be assembled using the same TSM units, as defined in Section 3. Figure 18 illustrates a concept of such a TSM by depicting imaginary facets and edges (lines of SLEs are omitted for clarity). Side planes and connecting planes have been replaced with each other at the intermediate cross-section depicted in bold lines.

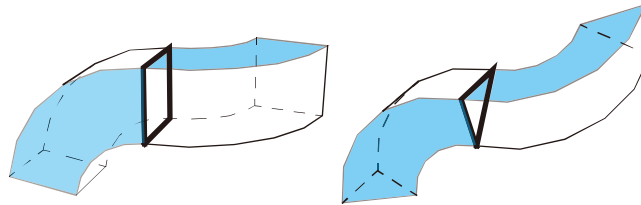


**Fig. 18.** Change in directions of three-dimensionally twisting TSM.

(Colored facets represent one of the side planes).

Because a triangular TSM unit contains two identical side planes, the facets cannot rotate if the three sides of the triangular cross-section have different lengths. Consequently, the triangular TSMs that extend three-dimensionally can be designed with only equilateral-triangular cross-sections. The rotation angle can be either  $120^\circ$  or  $240^\circ$ , as shown in Fig. 19, which enables a drastic change in the extension direction. Figure 20 shows the deployment sequence of the triangular TSM with 12 units, of which the facets were rotated twice. For clarity,

all the imaginary facets are depicted in white, pSLEs by black lines, and mSLEs by red lines. Such a three-dimensional extension was not achieved in previous studies, and it widens the deployability of TSMs.

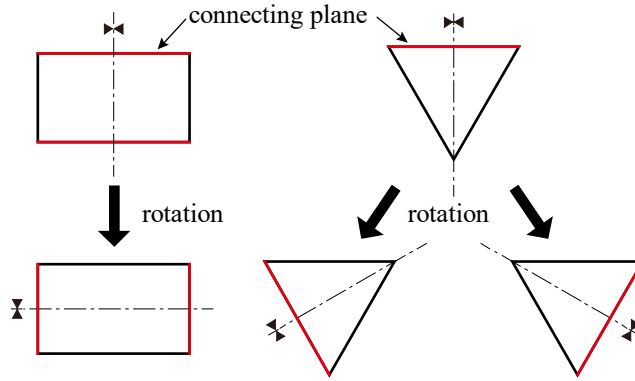


**Fig. 19.** Cross-sections before and after rotation.

(Red lines represent the sides of the connecting planes).

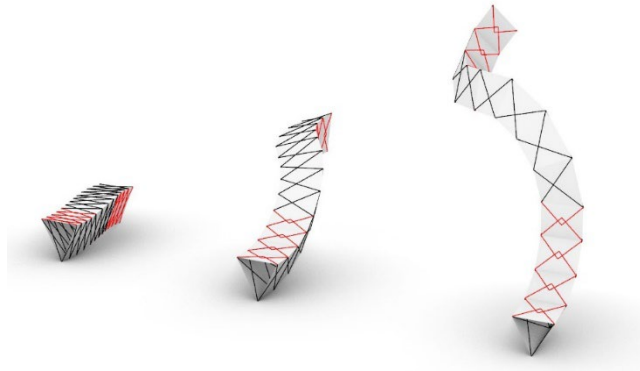


**Fig. 20.** Deployment sequence of a three-dimensionally extendable triangular TSM.

In contrast, a rectangular TSM can be rotated by only  $90^\circ$ ; however, its cross-section is not necessarily square. A rectangular TSM with square cross-sections can be assembled by setting  $k = 1$ . In addition, a rectangular TSM with a constant width–thickness ratio is also eligible. If the constant width–thickness ratio before the rotation is  $k$ , the ratio after the rotation,  $k'$ , should be equal to  $1/k$ ; if the lengths of pSLEs and mSLEs before the rotation are  $L = L_0$  and  $l = kL_0$ , respectively, those after the rotation are  $L' = kL_0$  and  $l' = L_0$ , respectively. Figure 21 shows the

deployment sequence of a rectangular TSM; the number of units is nine,  $k = 0.6$ , and the facets are rotated twice.

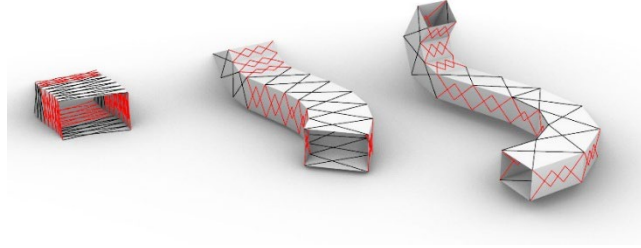


**Fig. 21.** Deployment sequence of a three-dimensionally extendable rectangular TSM.

## 4.2. Connections

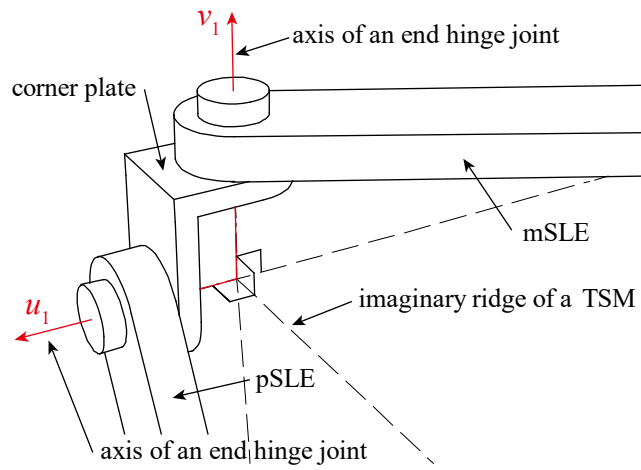
In the previous discussion, the bars and connections were all modeled with ideal lines and points, respectively. However, the finite sizes of the bars and joints and their details need to be carefully considered because they affect the possibility of the deployment of physical models. Nevertheless, as this study does not aim to pursue technical design details, we briefly describe one of the most straightforward solutions to incorporate the sizes of the bars and joints.

As mentioned in Section 3.1, a rectangular TSM must connect its side planes and connecting planes with joints that maintain right angle. A simple joint using a corner plate is shown in Fig. 22(a), where the hinge axes  $u_1$  and  $v_1$  are orthogonal. Because pSLE and mSLE are shifted from their ideal positions in the direction perpendicular to their planes, the bar lengths remain unchanged. In addition, this type of joint does not increase the DOF of the mechanism (You and Chen, 2012; Zhao et al., 2009).

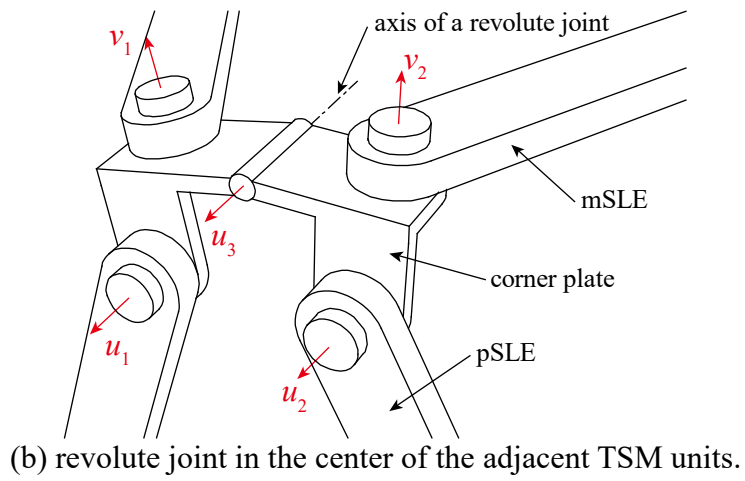
The more perplexing problem is that the angles between adjacent connecting planes vary continuously. Hence, the mSLEs of adjacent units cannot connect directly with conventional revolute joints. Spherical joints may settle the problem; however, they are not practical in terms of cost. One of the solutions to avoid these problems is to separate the adjacent units so that

their unit lines are parallel and assign revolute joints at their centers, as shown in Fig. 23. The details of this connection are shown in Fig. 22(b), where the hinge axes  $u_1$ ,  $u_2$ , and  $u_3$  are parallel. This operation changes the curved geometry from the original; however, the change is small when the joint size is small compared to the bar lengths. In addition, the movement of the mechanism is not obstructed. Note that because three hinges are arranged in parallel in the figure, the DOF of the TSM may seem to increase with an additional sway mode. However, this can be avoided because the corner plate shown in Fig. 22(b) can transfer out-of-plane bending moments of mSLEs. Figure 24 illustrates how the mSLEs prevent such extra movements, cooperating with the corner plates. We also evaluated the DOF of the TSM by computation using singular value decomposition of the equilibrium matrix (Pellegrino, 1993; Ohsaki et al., 2016; Tsuda et al., 2013) and confirmed that the DOF is one. A summary of the method is described in Appendix A.

Figure 25 shows the deployment sequence of small physical models of the TSMs assembled with joints fabricated using a 3D printer. We confirmed that the TSMs deploy smoothly by controlling the locations of the two points. However, it cannot be folded or deployed entirely because of the finite size of the bars and joints, primarily because of the existence of intermediate revolute joints. Thus, more adequate connections should be devised in future work. Note that this model is made to evaluate deployability and is not made with materials or components that can be applied to loading tests. Although this paper focuses on the geometry of the mechanism but not stresses in the structure, Appendix B briefly describes the stress analysis of a small TSM model and gives an overview of its mechanical properties. Further research is needed to assess the stresses in the members and connections after deployment to create a robust structure for practical use, especially for large and complex structures, such as the spiral model under various loading conditions.



(a) Corner plate of the rectangular TSM



(b) revolute joint in the center of the adjacent TSM units.

**Fig. 22.** Details of joints.

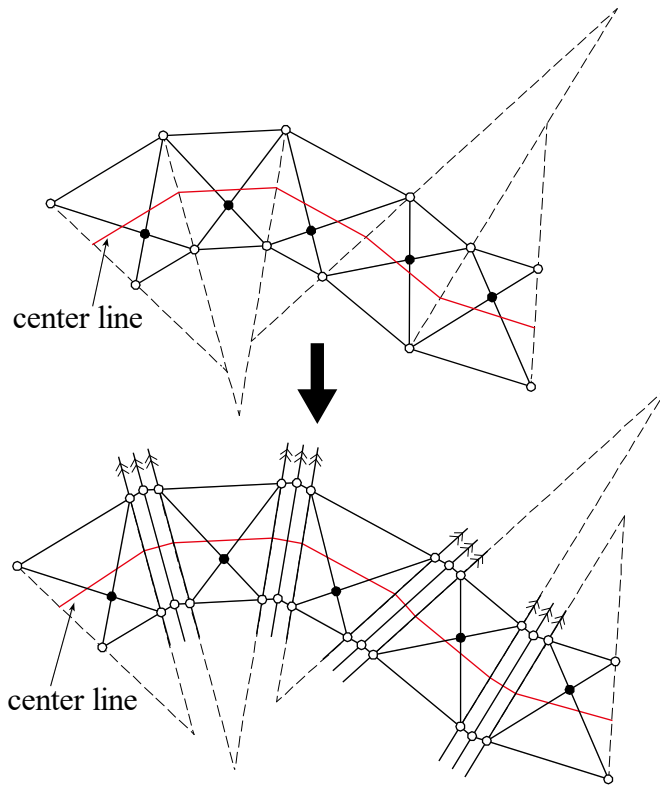


**Fig. 23.** Change of curve from the parallel shift of adjacent units.

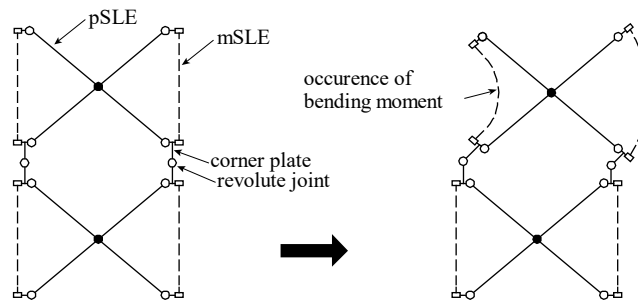
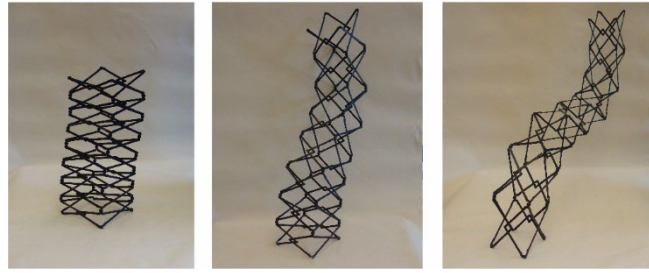
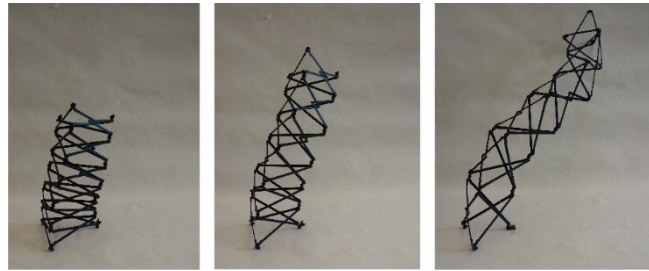


**Fig. 24.** Out-of-plane rigidity of mSLEs.



(a) Two-dimensionally winding rectangular-TSM



(b) Three-dimensionally twisting triangular-TSM



(c) Close-up photo of joints

**Fig. 25.** Sequence of small physical models.

## 5. Conclusions

This paper describes the composition of the pantographic tubular scissor mechanisms, called TSMs, extending two- or three-dimensionally with compound curves. The TSMs are composed of SLEs on their surrounding facets, while their internal space is vacant. To form a winding profile, two pSLEs—polar scissor units, which consist of two straight bars eccentrically connected to a revolute joint, are arranged on the side planes of the TSM. These pSLEs are connected with mSLEs—translational scissor units, which consist of symmetrically assigned elements with multi-tiers or rows, on the connecting planes.

This study focuses on the geometric design of TSMs with rectangular and triangular cross-sections. Because the TSMs are composed of SLEs on all their surrounding facets, their cross-sectional shape and size change continuously. Therefore, we derived the constraints on the geometrical properties so that the TSMs can keep their outlines of the cross-section similar during deployment.

The constraint equations are derived with ideal lines and points, while the sizes of the elements and connections are neglected. However, connection details should be designed to satisfy the constraint equations without increasing the DOF of the mechanism. Therefore, this study presents an example of a simple connection. Physical models were fabricated to verify their deployability. They deploy smoothly by controlling the locations of the two points and demonstrate single-DOF. It should be noted that they cannot be folded or deployed entirely because of the interference in parts of the connections. Therefore, more sophisticated connections should be investigated in future studies.

This paper focuses on the geometry of TSMs and their mobility without discussing their mechanical performance in depth. However, the mechanical properties of the structures and the strength of the members and connections should be further investigated to utilize TSMs in gravity-dominated environments, especially for large and complex structures.

The high transformability of the proposed TSMs can be applied to deployable structures such as extendable masts, retractable roof structures, and space antennas. In addition, because TSMs are vacant internally and can connect two spatially separated spots, they can also serve as movable pedestrian bridges and lifters. Besides, the cross-sectional shapes can be tuned as desired. Therefore, it is necessary to determine the appropriate compositions and lengths of the bars to design assemblies that meet the purpose and geometrical conditions. In future work, we plan to develop an optimization method for this.

## Funding

This work was supported by JSPS KAKENHI (grant number 19K04714).

## Acknowledgment

We would like to thank Editage (www.editage.com) for English language editing.

## Appendix

### A. Evaluation of DOF by singular value decomposition of the equilibrium matrix

The method to construct equilibrium matrices of mechanisms is addressed, and the DOF is evaluated using singular value decomposition of the equilibrium matrices (Tsuda et al., 2013). An assembly with  $n_m$  members,  $n_n$  nodes, and  $n_f$  fixed displacements is assumed. Figure A.1 shows member  $k$  that connects nodes  $i$  and  $j$ , including the local member coordinates  $(x, y, z)$ , global coordinates  $(X, Y, Z)$ , and member-end forces in both ends. We assume no load is distributed along the member. Then, each member has six independent components of member-end forces, denoted by  $\mathbf{f} = [N^{(k)}, T^{(k)}, M_{yi}^{(k)}, M_{zi}^{(k)}, M_{yj}^{(k)}, M_{zj}^{(k)}]^T$ , because four shear forces ( $Q_{yi}^{(k)}$ ,  $Q_{zi}^{(k)}$ ,  $Q_{yj}^{(k)}$ ,  $Q_{zj}^{(k)}$ ) can be obtained from bending moments and member length.

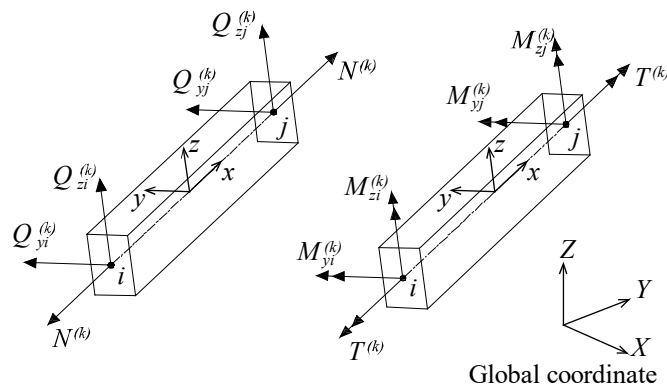


**Fig. A.1.** Definition of the coordinate systems and member-end forces.

The member-end forces of all members are transformed from the local member coordinate

to the global coordinate. Equilibrium equations with these forces and external nodal forces are formulated for each node;  $\mathbf{F}$  denotes the vector of all member-end forces, which has  $m$  ( $= 6n_m$ ) components;  $\mathbf{P}$  denotes the nodal load vector except fixed nodes, which has  $n_p$  ( $= 6n_n - n_f$ ) components. If some member-end forces are released using end hinges, the equilibrium equation is written as follows:

$$\begin{bmatrix} \mathbf{C} \\ \mathbf{H} \end{bmatrix} \mathbf{F} := \mathbf{B}\mathbf{F} = \begin{bmatrix} \mathbf{P} \\ \mathbf{0} \end{bmatrix}, \quad (\text{A.1})$$

where equilibrium matrix  $\mathbf{C}$  is an  $n_p \times m$  rectangular matrix; matrix  $\mathbf{H}$  contains one at the components corresponding to the released member-end force and zero at the remaining components. When the number of released forces at end hinges is  $h$ ,  $\mathbf{H}$  is an  $h \times m$  rectangular matrix. Extended equilibrium matrix  $\mathbf{B}$  is an  $n$  ( $= n_p + h$ )  $\times m$  rectangular matrix. The rank of  $\mathbf{B}$  is assumed to be  $r$ . By using the singular value decomposition of  $\mathbf{B}$ , we can obtain

$$\mathbf{B} = \mathbf{S}\mathbf{V}\mathbf{R}^T, \quad (\text{A.2})$$

where  $\mathbf{V}$  is an  $n \times m$  rectangular diagonal matrix with  $r$  positive components at the leading diagonal and zero at the remaining components;  $\mathbf{S}$  and  $\mathbf{R}$  are the matrices consisting of left-singular vectors  $\mathbf{S}_j$  and right-singular vectors  $\mathbf{R}_j$ , respectively. Figure A.2 illustrates the matrix components of the singular value decomposition of matrix  $\mathbf{B}$  with rank  $r$ .

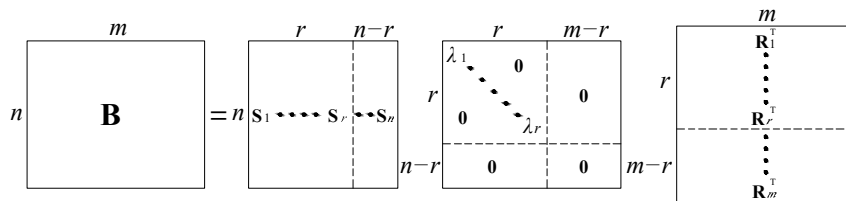


**Fig. A.2.** Matrix components of the singular value decomposition of matrix  $\mathbf{B}$ .

(The nonzero singular values are  $\lambda_i$  ( $i = 1 - r$ ). The letters to the left and top of the matrix indicate the number of rows and columns, respectively.)

Because  $\mathbf{S}$  and  $\mathbf{R}$  are orthogonal matrices, the following equations can be obtained from Eq. (A.2). When  $r$  is less than  $m$ ,  $p (= m-r)$  vectors of  $\mathbf{R}_j$  satisfy

$$\mathbf{B}\mathbf{R}_j = \mathbf{0}. \quad (\text{A.3})$$

Additionally, when  $r$  is less than  $n$ ,  $q (= n-r)$  vectors  $\mathbf{S}_j$  satisfy

$$\mathbf{B}^T\mathbf{S}_j = \mathbf{0}. \quad (\text{A.4})$$

From Eqs. (A.1) and (A.3),  $\mathbf{R}_j$  is the mode of the self-equilibrium force that exists without external loads  $\mathbf{P}$ . Hence,  $p$  is the degree of static indeterminacy.

Next, the meaning of left-singular vectors  $\mathbf{S}_j$  is discussed;  $\mathbf{U}$  denotes node displacements, and  $\boldsymbol{\theta}$  denotes rotational angles of the hinges relative to the nodes. Assume that the member-end deformation vector  $\mathbf{d}$  is expressed using  $\mathbf{U}$  and  $\boldsymbol{\theta}$  as follows.

$$\mathbf{d} = \mathbf{D}\mathbf{U} + \mathbf{G}\boldsymbol{\theta} \quad (\text{A.5})$$

Considering the virtual work with the virtual displacement  $\mathbf{U}$  and the virtual deformation  $\mathbf{d}$  in the framework where the external force  $\mathbf{P}$  and the member force  $\mathbf{F}$  are generated, we can obtain  $\mathbf{F}^T\mathbf{d} = \mathbf{F}^T(\mathbf{D}\mathbf{U} + \mathbf{G}\boldsymbol{\theta}) = \mathbf{P}^T\mathbf{U}$ . Because  $\mathbf{U}$  and  $\boldsymbol{\theta}$  can be considered independent virtual displacements and virtual hinge rotation angles, respectively, we obtain  $\mathbf{D}^T\mathbf{F} = \mathbf{P}$  and  $\mathbf{G}^T\mathbf{F} = \mathbf{0}$ . Therefore, we can obtain  $\mathbf{D} = \mathbf{C}^T$  and  $\mathbf{G} = \mathbf{H}^T$  from these relations and Eqs. (A.1). The vector  $\mathbf{S}_j$  can be expressed as  $\mathbf{S}_j = [\mathbf{C}\mathbf{S}_j^T \ \mathbf{H}\mathbf{S}_j^T]^T$ , where  $\mathbf{C}\mathbf{S}_j$  and  $\mathbf{H}\mathbf{S}_j$  are blocks corresponding to matrices  $\mathbf{C}$  and  $\mathbf{H}$ , respectively. Therefore, Eq. (A.4) can be rewritten as

$$\mathbf{D} \ \mathbf{C}\mathbf{S}_j + \mathbf{G} \ \mathbf{H}\mathbf{S}_j = \mathbf{0}. \quad (\text{A.6})$$

From Eqs. (A.5) and (A.6), the vector  $\mathbf{S}_j$  satisfies  $\mathbf{d} = \mathbf{0}$ . Therefore,  $\mathbf{S}_j$  that satisfies Eq. (A.4) is the mode of an unstable mechanism. Hence,  $q$  corresponds to the degree of kinematic indeterminacy, i.e., DOF of the mechanism.

The singular value analyses for the two-unit linear TSMs shown in Fig. A.3(a) are performed to verify the effect of the connections on mobility. The connections are the three types shown in Figure A.3(b): Type 1 is an ideal connection without any additional hinges; Type

2 contains the connections representing Fig. 22(b); Type 3 contains hinges at both ends of the connecting plate. To prevent rigid body motions, the boundary displacements are fixed in the  $X$ ,  $Y$ , and  $Z$  directions for node A, fixed in the  $Y$  and  $Z$  directions for node B, and fixed in the  $Z$  direction for node C. MATLAB R2019b (MathWorks, 2019) is used for calculation.

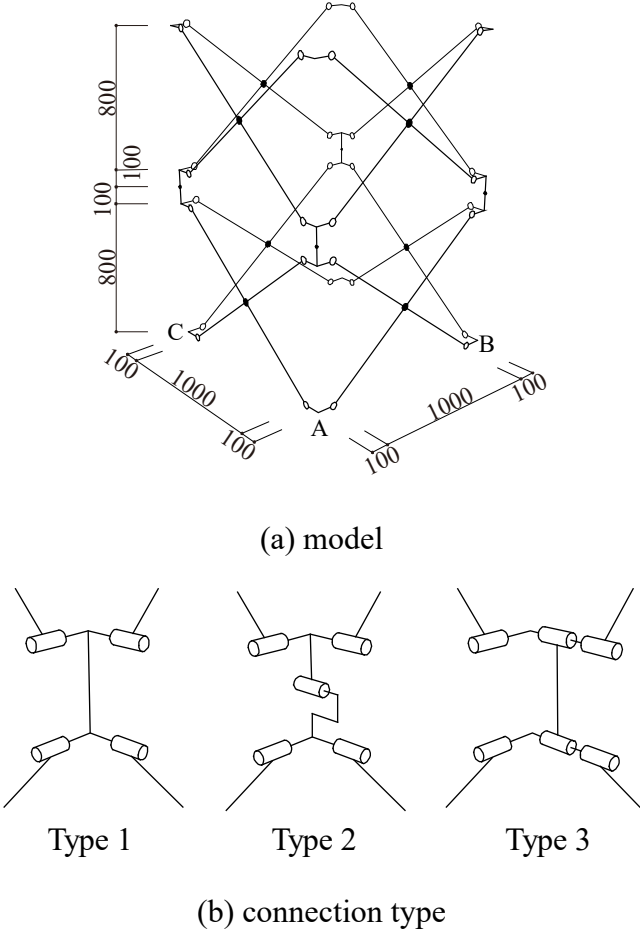


**Fig. A.3. Calculation model.**

The results of the analyses are listed in Table A.1. The unstable mode for Type 1 and Type 2 is the expansion mode shown in Fig. A.4(a). Type 3 contains an additional sway mode shown in Fig. A.4(b). Therefore, connections that can transmit out-of-plane bending moments of SLEs are required. Note that yielding of members and connections in a mechanism can cause

instability due to increased DOF; however, partial yielding of a TSM does not necessarily lead to total collapse because it has large degrees of static indeterminacy, as shown in Table A.1.

Table A.1. Results of singular value analyses.

Type	DOF	Degree of static indeterminacy
1	1	39
2	1	35
3	2	32

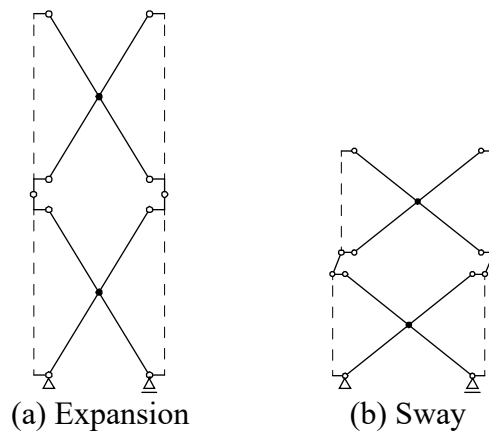
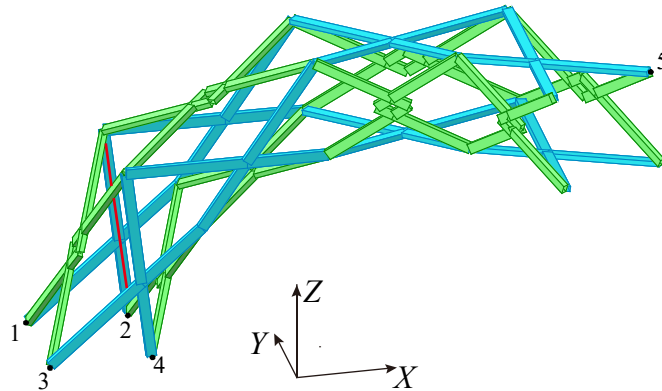


Fig. A.4. Mode of unstable mechanism.

## B. Stress analysis example of TSM

Stress analysis of a three-dimensionally curved TSM is described below to overview its basic mechanical properties. The model in Fig. B.1 consists of four identical units, rotated once at the midpoint. Each unit has a square cross-section with  $L = 2000$  and  $l = 1000$ ;  $e = 0.6$ ;  $\beta_S$  of the left and right mSLEs are 0.2247 and  $-0.1835$ , respectively;  $\theta$  is  $60^\circ$ . The material is steel (Young modulus is 205 GPa), and all members have the same box section BX-125 $\times$ 40 $\times$ 2.3 (the cross-sectional area is 724.2 mm<sup>2</sup>; the section modules are  $2.09 \times 10^4$  and  $1.08 \times 10^4$  mm<sup>3</sup>). The strong axis of the cross section is perpendicular to each SLEs plane. The size of the connection is not considered. Four nodes (1, 2, 3, and 4) are pin supported. Node 5 is located at the tip of this

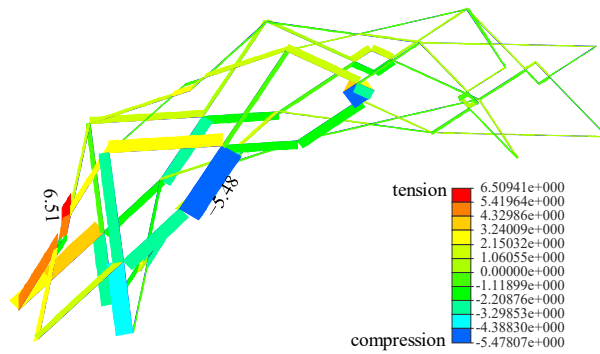
cantilever structure. The global coordinate of nodes 1 and 5 are (0, 0, 0) and (5.58 m, -2.63 m, 3.35 m), respectively. The stress analysis under the steel self-weight (total weight is 3.77 kN) was carried out using the finite element analysis software Midas iGen ver. 845 R2 (Midas Information Technology, 2015).



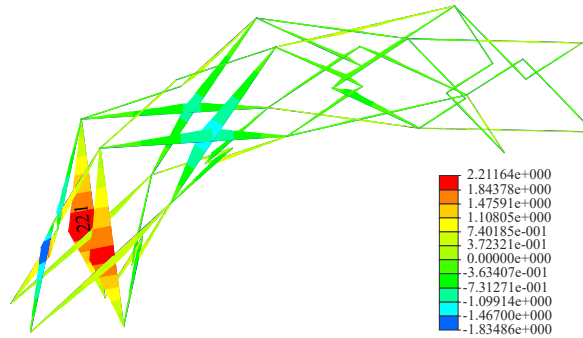
**Fig. B.1.** Stress analysis model.

(pSLEs are blue, and mSLEs are green.)

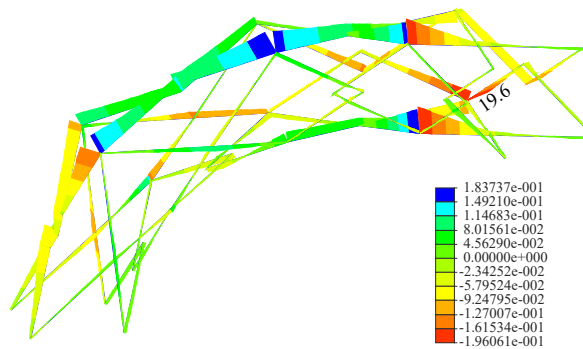
The stress analysis results are shown in Fig. B.2. The maximum stress occurred in the member marked with red in Fig. B.1 and is 121 MPa (axial stress = 3.88 MPa, in-plane bending stress = 106 MPa, and out-of-plane bending stress = 11.8 MPa). The deformation at node 5 is 64.9 mm (12.8, -24.1, and -58.9 mm in the  $X$ ,  $Y$ , and  $Z$  directions, respectively). The load is mainly transferred by in-plane bending moments of SLEs. In the stress analysis, the cross section is assumed to be uniform in shape along the length of the element; however, it is more efficient to use a variable cross section according to the in-plane bending moment gradient. Note that this analysis neglects the size of the joints, whereas taking this into account would result in additional eccentric stresses. In addition, although this analysis uses steel materials, the use of lighter and stronger materials, such as carbon fiber reinforced plastic (CFRP), will lead to the realization of even larger structures.



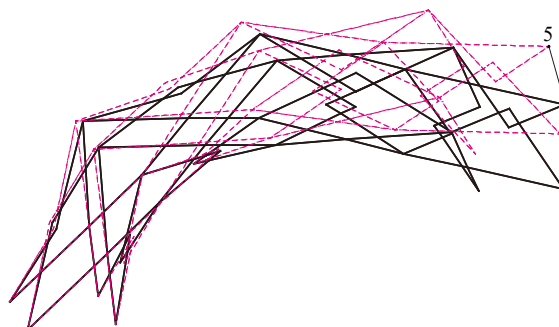
(a) Axial Force (unit = kN)



(b) In-plane bending moment (unit = kNm)



(c) Out-of-plane bending moment (unit = kNm)



(d) Displacement (scale factor = 10)

**Fig. B.2.** Stress analysis results.

(Only maximum member forces are given in each figure.)

## References

- Alegria Mira, L., Thrall, A.P., De Temmerman, N., 2014. Deployable scissor arch for transitional shelters. *Autom. Constr.* 43, 123–131. DOI:[10.1016/j.autcon.2014.03.014](https://doi.org/10.1016/j.autcon.2014.03.014).
- Hario, I., Nakazawa, M., Tanaka, Y., Tanikura, I., Ono, S., 2013. Development of a prototype deployable bridge based on origami skill. *Autom. Constr.* 32, 104–111. DOI:[10.1016/j.autcon.2013.01.012](https://doi.org/10.1016/j.autcon.2013.01.012).
- Atake, K., 2000. ATAKE's structure—new variations of the scissors technique. *Mobile and Rapidly Assembled Structures III*, pp. 143–154. WIT Press.
- Babaei, M., Sanaei, E., 2009. Geometric and structural design of foldable structures. *Proceedings of the IASS Symposium 2009, Valencia*.
- De Temmerman, 2007. N. Design and Analysis of Deployable Bar Structures for Mobile Architectural Applications. Ph.D. Dissertation. Vrije Universiteit Brussel.
- Escrig, F., 1985. Expandable space structures. *Int. J. Space Struct.* 1, 79–91. DOI:[10.1177/026635118500100203](https://doi.org/10.1177/026635118500100203).
- Escrig, F., Valcarcel, J.P., 1993. Geometry of expandable space structures. *Int. J. Space Struct.* 8, 71–84. DOI:[10.1177/0266351193008001-208](https://doi.org/10.1177/0266351193008001-208).
- Glisic, B., Adriaenssens, S., Szerzo, P., 2013. Structural analysis and validation of a smart pantograph mast concept. *Comput.-Aided Civ. Infrastruct. Eng.* 28, 651–665. DOI:[10.1111/mice.12013](https://doi.org/10.1111/mice.12013).
- Hanaor, A., Levy, R., 2001. Evaluation of deployable structures for space enclosures. *Int. J. Space Struct.* 16, 211–229. DOI:[10.1260/026635101760832172](https://doi.org/10.1260/026635101760832172).
- Hoberman, C., 1990. Reversibly expandable doubly-curved truss structure. US Patent number 4942700.
- Kwan, A.S.K., You, Z., Pellegrino, S., 1993. Active and passive cable elements in deployable/retractable masts. *Int. J. Space Struct.* 8, 29–40.

DOI:[10.1177/0266351193008001-204](https://doi.org/10.1177/0266351193008001-204).

Langbecker, T., 1999. Kinematic analysis of deployable scissor structures. *Int. J. Space Struct.* 14, 1–15. DOI:[10.1260/0266351991494650](https://doi.org/10.1260/0266351991494650).

Langbecker, T., Albermani, F., 2001. Kinematic and non-linear analysis of foldable barrel vaults. *Eng. Struct.* 23, 158–171. DOI:[10.1016/S0141-0296\(00\)00033-X](https://doi.org/10.1016/S0141-0296(00)00033-X).

Maden, F., Akgün, Y., Kiper, G., Gür, Ş, Yar, M., Korkmaz, K., 2019. A critical review on classification and terminology of scissor structures. *J. Int. Assoc. Shell Spat. Struct.* 60, 47–64. DOI:[10.20898/j.iass.2019.199.029](https://doi.org/10.20898/j.iass.2019.199.029).

Maden, F., Korkmaz, K., Akgün, Y., 2011. A review of planar scissor structural mechanisms: geometric principles and design methods. *Archit. Sci. Rev.* 54, 246–257. DOI:[10.1080/00038628.2011.590054](https://doi.org/10.1080/00038628.2011.590054).

MathWorks, 2019. MATLAB User's Manual Version R2019b.

Midas Information Technology, 2015. Midas iGen User's Manual Version 2015.

Ohsaki, M., Tsuda, S., Miyazu, Y., 2016. Design of linkage mechanisms of partially rigid frames using limit analysis with quadratic yield functions. *Int. J. Solids Struct.* 88–89, 68–78. DOI:[10.1016/j.ijsolstr.2016.03.023](https://doi.org/10.1016/j.ijsolstr.2016.03.023).

Pellegrino, S., 1993. Structural computations with the singular value decomposition of the equilibrium matrix. *Int. J. Solids Struct.* 30, 3025–3035. DOI:[10.1016/0020-7683\(93\)90210-X](https://doi.org/10.1016/0020-7683(93)90210-X).

Pinero, E.P., 1965. Three-dimensional reticular structure. US Patent number 3185164.

Raskin, I., 1998. Stiffness and stability of deployable pantographic columns. Ph.D. Dissertation. The University of Waterloo.

Roovers, K., De Temmerman, N., 2017. Deployable scissor grids consisting of translational units. *Int. J. Solids Struct.* 121, 45–61. DOI:[10.1016/j.ijsolstr.2017.05.015](https://doi.org/10.1016/j.ijsolstr.2017.05.015).

Rosenberg, D., 2010. Indeterminate Architecture: Scissor-Pair Transformable Structures. Delft

School of Design Journal. Issue # 6 Digitally-Driven Architecture. DOI:  
[10.7480/footprint.4.1.717](https://doi.org/10.7480/footprint.4.1.717).

Tsuda, S., Ohsaki, M., Kikugawa, S., Kanno, Y., 2013. Analysis of stability and mechanism for frames with partially rigid connections. *Journal of Structural and Construction Engineering (Transactions of AIJ)* 78, 791–798. (in Japanese). DOI:[10.3130/aijs.78.791](https://doi.org/10.3130/aijs.78.791).

You, Z., Chen, Y., 2012. *Motion Structures*. Spon Press.

You, Z., Pellegrino, S., 1996. Cable-stiffened pantographic deployable structures part 1: triangle mast. *AIAA J.* 34, 813–820. DOI:[10.2514/3.13144](https://doi.org/10.2514/3.13144).

Zhao, J., Chu, F., Feng, Z.-J., 2009. The mechanism theory and application of deployable structures based on SLE. *Mech. Mach. Theory*, 44, 324–335. DOI:[10.1016/j.mechmachtheory.2008.03.014](https://doi.org/10.1016/j.mechmachtheory.2008.03.014).